We greatly appreciate the insightful reviews by the reviewers. Below are our responses (in red) to each of the review comments (in black)

Response to Reviewer 1

Specific comments:
Representation of sea ice concentration anomalies with 9 SOM spatial patterns (nodes, provided in Fig. 1) was selected. It is stated that results are similar with larger numbers of nodes, while smaller numbers are less representative. It is not clear how the spatial correlation coefficient (Table 1) was calculated however, and a change from 0.59 (2x4 nodes) to 0.64 (3x3 nodes) does not seem 'large' as stated on line 84.

The spatial correlation values in Table 1 are obtained by two steps. First, for each autumn, spatial correlation between the sea ice anomaly pattern and the best matching SOM pattern is calculated (Lee and Feldstein, 2013). Second, the spatial correlations for all 38 autumns are averaged to obtain the mean spatial correlations shown in Table 1. These steps are repeated for the 8 pre-determined SOM grids in Table 1.

The change from 0.59 to 0.64 is not large, but it is the largest gain between any two grids among the 8 grids tested. The choice of the grid is, admittedly, subjective. Obviously, higher spatial correlation can be achieved with larger grids. The 3x3 grid is able to capture the main variability pattern at the sacrifice of some details that can be depicted by larger grids.

We have added clarification about the values in Table 1 and further justification of the choice of the grid. (lines 97-106)

For each of the 38 seasons available the best-matching node is tabulated (Fig 2). The 'frequency of occurrence' is defined as the number of times a pattern is thus selected, divided by 38: thus both node 1 and node 9 have a frequency of occurrence of 23.7% (9/38) in Fig. 1.Nodes 1 and 9 have similar spatial distribution but opposite sign: node 9 (positive anomalies) is prominent early in the analysed period, and node 1 (negative anomalies) late in the period. Fig. 3 shows trends associated with each node: this seems to be the node spatial pattern multiplied by a rate. (It is not clear how the rate is determined: possibly temporal linear regression of the projections of each pattern each season?) Nodes 1 and 9 are the main contributors.

The reviewers are correct about how the frequencies of occurrences and the trends or the rates of the change are determined.

We have added clarification for these calculations (lines 109-110)

Fig. 4 illustrates how much of the total observed trend is associated with the SOM nodes. (It is not clear how this is calculated, but the text states about 60% in all is associated with the selected SOM nodes.)

The contribution of each SOM pattern to trends in Arctic sea ice concentration is calculated by the product of each SOM pattern and the rate, defined as temporal linear regression of the number of the projections of each pattern for each autumn. The sum of contributions from each node presents the total observed trend associated with the SOM nodes.

The 60% is estimated by the ratios of residual trends to the total trends that range from 10 to 90% across grid points with statistically significant trends. (lines 108-111)

This has been clarified in the manuscript

Composites of sea surface temperature anomalies and various atmospheric quantities (anomalies from ERA-interim: 500hPa geopotential height, 850hPa wind, surface air T, surface downward longwave radiation, surface-to-750hPa water vapour) are made using years indicated in Fig. 2 for node 1 (2007-2013, 2015-2016), and, separately, for node 9 (1980-1982, 1986-1989, 1992, 1996). Effectively the SOM analysis provides the basis for these composites, which are illustrated in Figs. 5-7. The composites are likely quite similar to composites of years when autumnal Arctic sea ice coverage was high versus low according to various other criteria: this should be discussed. The authors claim SOM allows 'better depiction of atmospheric circulation patterns that have significant impact on sea ice trends' (line 175), but no evidence is provided to support this claim, and this is a major weakness of this article.

The following paragraph and a new figure (Figure 8) have been added that compares SOM-based composites with typical time-series based composite approach.

The SOM-based composites in the above discussion, which are made using years indicated (Fig. 2) by the occurrences for Node 1 (2007-2013, 2015-2016), and, separately, for node 9 (1980-1982, 1986-1989, 1992, 1996), are compared to composites of years of high (before 2000) and low (after 2000) Arctic sea ice coverage according to the Autumn Arctic sea ice time series (Figure 8). The composited SST patterns over the North Pacific are almost a mirror image to each other, indicating a positive (negative) phase PDO before (after) 2000 (Fig. 8). On the other hand, the composited SST patterns corresponding to Node 1 and Node 9 are not symmetrical (Fig. 5). Similar situations occur over North Atlantic. The magnitude and significant level of SOM-based SST composites in Fig. 5 are also higher than the time-series-based composites in Fig. 8. Similarly, in mid-latitudes, the composites of the anomalous 500hPa geopotential heights before and after 2000 are nearly symmetrical (Fig. 8) and the significant level and amplitude of the wave train are also lower than those in Fig. 5. At high latitudes, the anomalous atmospheric circulations in Fig. 8 show a mixed pattern of AO and AD and have no extreme centers. However, Fig. 5 exhibits clear AO and AD patterns and extreme centers, revealing more clearly the relationship between the anomalous sea ice concentration and anomalous atmospheric circulations. Based on these examples, the SOM-based composites allows for better depiction of atmospheric and SST conditions corresponding to sea ice anomaly patterns compared to typical time-series-based composite approach. (lines 211-227)

With a relatively small number of cases (9) in each composite, some discussion of whether the composites are dominated by a few 'extremes' should be provided.

The following paragraph, along with three new figures, has been added.

One drawback of the SOM-based composite is the relatively small number of composite members (Node 1 and Node 9 each has 9 members), which makes the composite more vulnerable to the influence of extreme cases. To examine this issue, the standard deviations of the SOM-based composites are compared to those of time-series-based composites that have much larger members (17 members for after-2000- composites and 21 members for before-2000-composites) and the results for the anomalous SST and 500-hPa height are shown in Figs. S1 and S2. The spatial patterns and magnitudes of the standard deviations are similar between the Node-1 and after-2000 composites and between Node-9 and before-2000 composites. The F-test indicates that except for small patches there are no statistically significant differences in the standard deviations between the small member SOM-based composites and

the large-member typical composites (Fig.3), suggesting it is unlikely the SOM-based composites are strongly influenced by extreme cases as a result of small composite members. (lines 228-239)
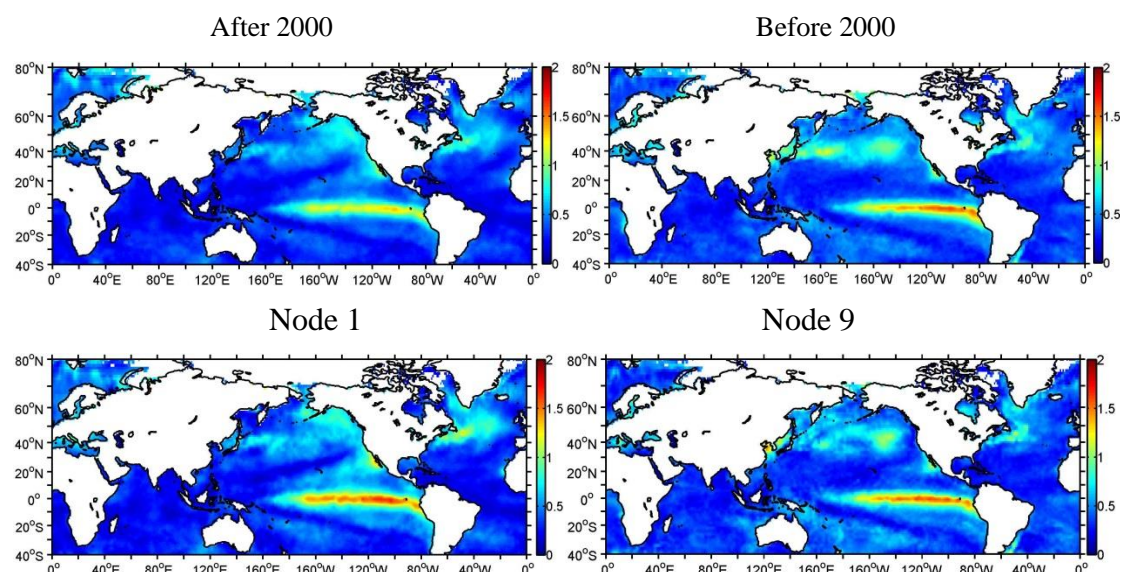
Figure S1 The standard deviations of composite SST for Nodes 1 and 9, and after and before 2000.
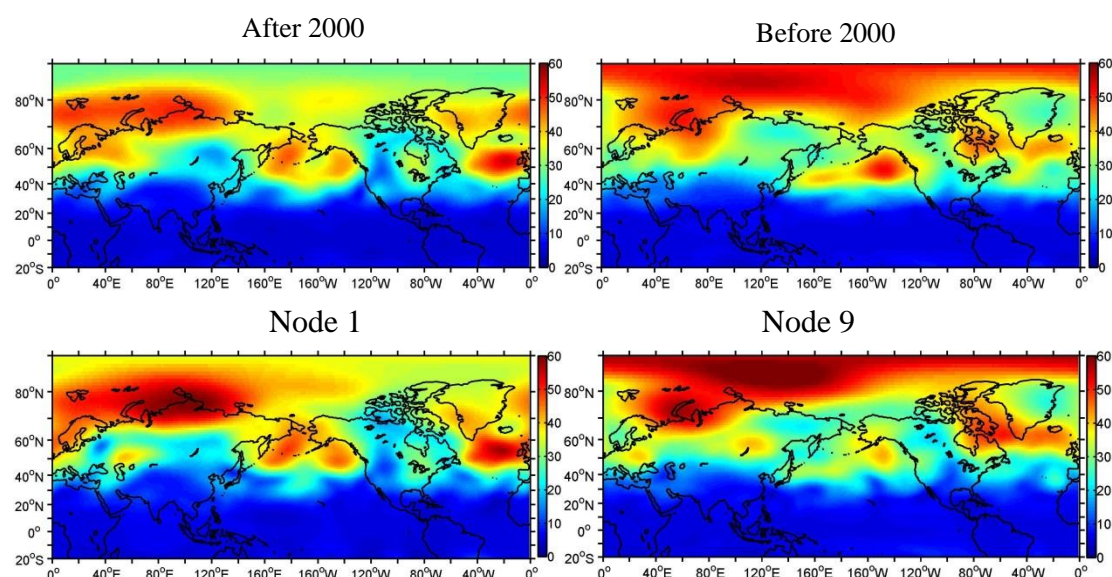

Figure S2 The standard deviations of composite 500-hPa height for Nodes 1 and 9, and after and before 2000.
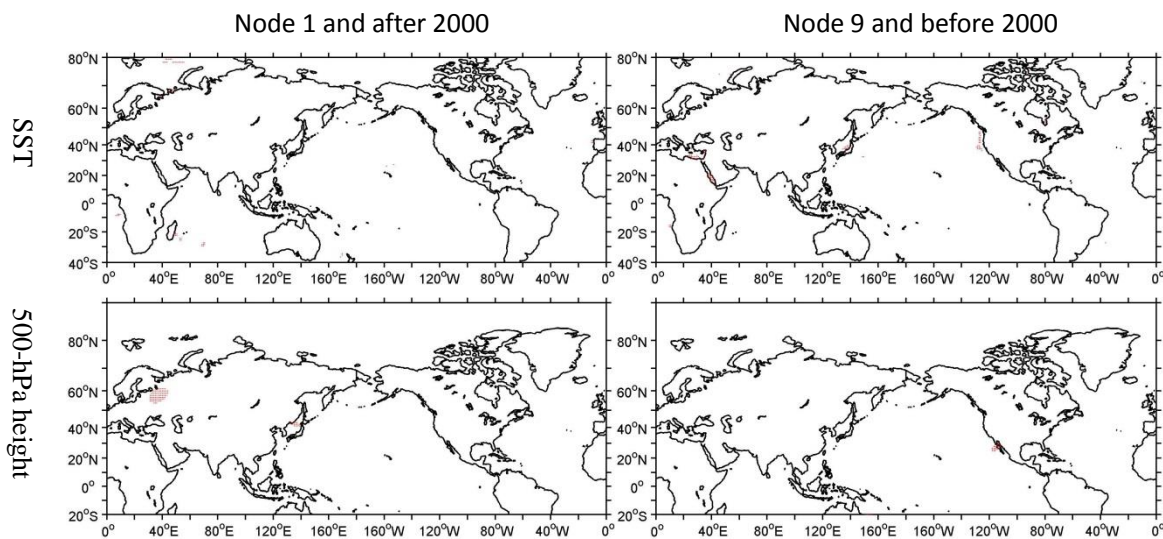
Figure S3 The significant test of standard deviation for SST and 500-hPa height between Node 1 and after 2000, and Node 9 and before 2000 using F test. Red dots denote above 95% confidence level.

The analysis is largely descriptive. Various features in the composites are noted that are consistent with Arctic changes: e.g. for node 1 there are influences that favour sea ice reduction. Although suggestive in appearance, it is not evident that the SST anomalies and geopotential height anomalies in Fig. 5 are related as described. A zonal wavenumber 2 wavetrain (lines 134, 152) is not obvious.

We have added OLR composite analysis to determine the source of the wave train and further explain the relationship between SST and geopotential height anomalies. The anomalous convection activity over the tropical western Pacific Ocean can excite a wave train that propagates northeastwards. Over the mid-latitude North Pacific, the different local interaction between anomalous SST and wave train for Nodes 1 and 9 leads to different and asymmetrical pattern in the high latitudes. (lines 157, 161-165, 186-191, Figure 5)

Regarding downward longwave radiation and water vapour, how reliable are the ERA analyses in the Arctic?

Ding et al. (2017) noted that the ERA-Interim analysis can represent reliably the observed circulation, radiation flux, temperature, and water vapour. Serreze et al. (2012) assessed humidity data from ERA-Interim analysis and found small bias of less than 8% at 1000 hPa for boreal autumn and smaller bias above 1000 hPa. Hence we considered ERA-Interim can represent reasonably well the observed downward longwave radiation and water vapour. (lines 73-76)

While the analyses demonstrate associated changes in sea ice and in SST and atmospheric circulation, they do not in themselves seem to indicate cause and effect, so it is difficult to draw conclusions regarding mechanisms. The 'important finding' relating sea ice changes to asymmetry in North Pacific SST anomalies (lines 184-188) is not well justified. The claim of 'large contributions from the decadal-scale natural climate variability to Arctic climate change' (lines 193-194) does not seem well justified.

We added OLR analysis to show the source of the wave train. Local and asymmetrical interactions of SST and the node of wave train produce anomalous atmospheric circulations over the mid-high latitudes, which are related to anomalous Arctic sea ice concentrations. (lines 157, 161-165, 186-191, Figure 5)

We agree that this and other analyses, which reveal the associations, do not demonstrate cause and effect. This is the major limitation of these types of climate diagnoses. We have softened the languages, e.g. important finding to major results, to reflect this point.

Other suggestions for technical corrections:

The term 'explained' is often used, but in the sense of statistical rather than physical explanation, which should be made clear.

We added 'in the statistical sense' in the sentence where 'explained' is used, or replaced the word 'explained' by 'is shown to be related'

The acronyms PDO, AMO, AD, AO are used without definition.

The definitions of PDO, AMO, AD, and AO were added in Dataset and Methods section (lines 65-70)

The title is rather misleading: the article is more about 'SST and atmospheric patterns associated with reductions in sea ice cover in recent decades'

The title is changed to 'The changes in sea-surface temperature and atmospheric circulation patterns associated with reductions in Arctic sea ice cover in recent decades'

The authors used the Self Organizing Maps (SOM) method to examine both the variability and trend of autumn Arctic sea ice over the past few decades. They found that about 60% of the recent autumn Arctic sea ice decline can be explained by 9 intrinsic modes, and specifically, SST anomalies over the North Pacific and North Atlantic, resulting atmospheric circulation and water vapor radiative processes.

The application of the SOM method to Arctic sea ice looks new to me and some interesting results are found. However, I have some major comments about this manuscript.

I would recommend publication in ACP when they are addressed.

Major comments:

1. About the number of nodes selected. Although the authors claimed that they chose 3x3 SOM grid because there is a large increase in correlation from 2x4 to 3x3, I feel the correlation increase looks pretty gradual to me and thus the choice of 3x3 is not very convincing. As the authors also claimed that "larger grids, : : :, do not alter the results and conclusions", I would suggest the authors include this information perhaps in the Supplementary Materials to better support the conclusions. Since, based on Table 1, increase of nodes after 3x5 does not seem to increase the correlation anymore, I would suggest the authors provide the results using 3x5.

As suggested by the reviewer, we now provide, as Supplemental Materials, the SOM patterns and their occurrence time series for the 3×5 grid (Figures S4and S5). As expected, with more nodes, the 3x5 grid depict more details and each node has smaller frequency compared to the 3x3 grid. However, the dominant nodes (also nodes 1 and 9) show nearly identical patterns as those in the 3x3 grid. Like the 3×3 grid, nodes 1 and 9 in the 3×5 grid make greater contributions to the trend in autumn Arctic sea ice than other nodes (Figure S6). Also as expected, the trend explained by nodes 1 and 9 in the 3x5 grid is smaller (46%) compared to 54% by the same two nodes in the 3×3 grid. (lines 147-153).
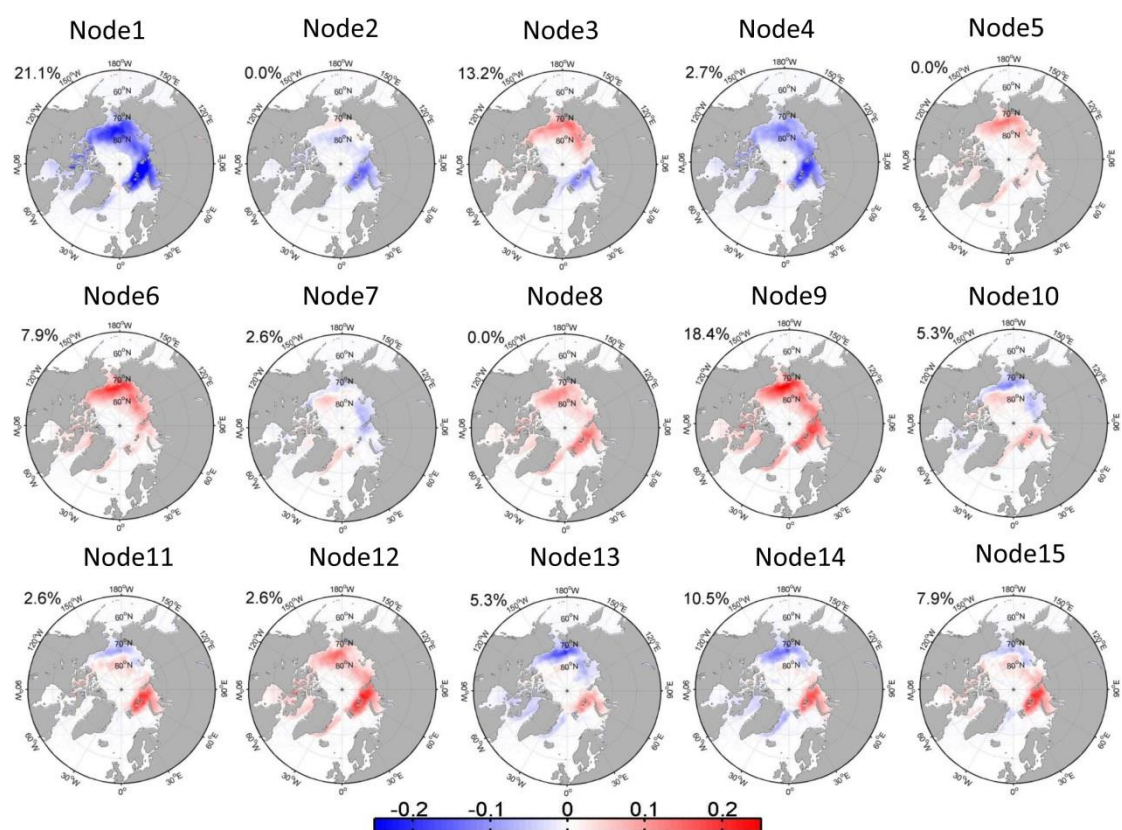
Figure S4 The SOM patterns of the anomalous autumn (September-November) Arctic sea ice concentration for a 3×5 grid for the 1979-2016 period. The percentages at the top left of each panel indicate the frequency of occurrence of the pattern.
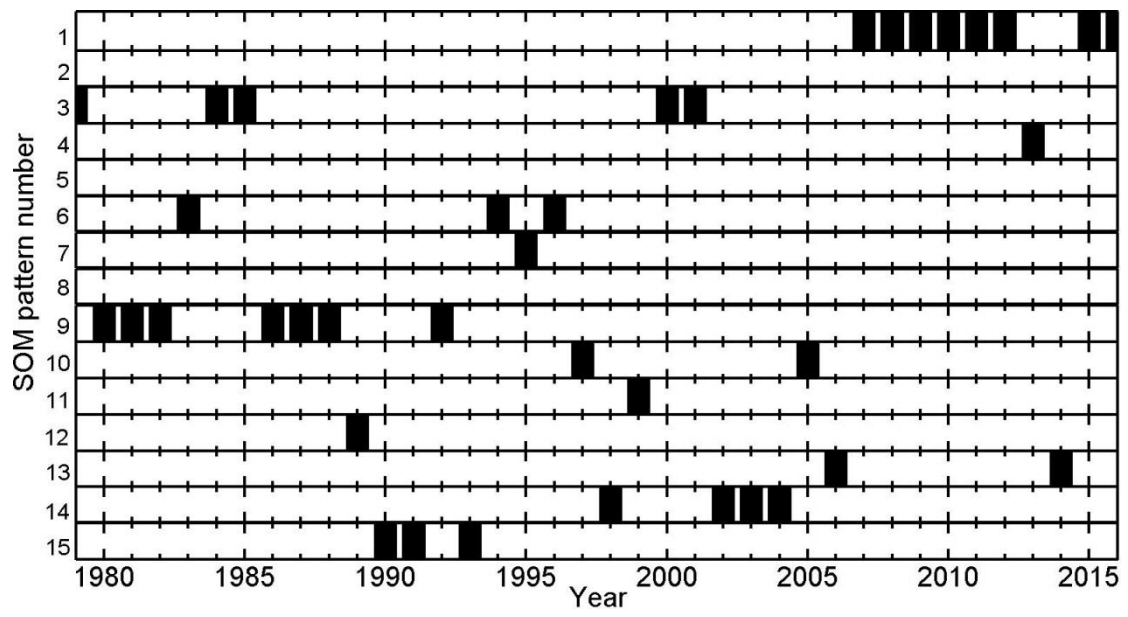
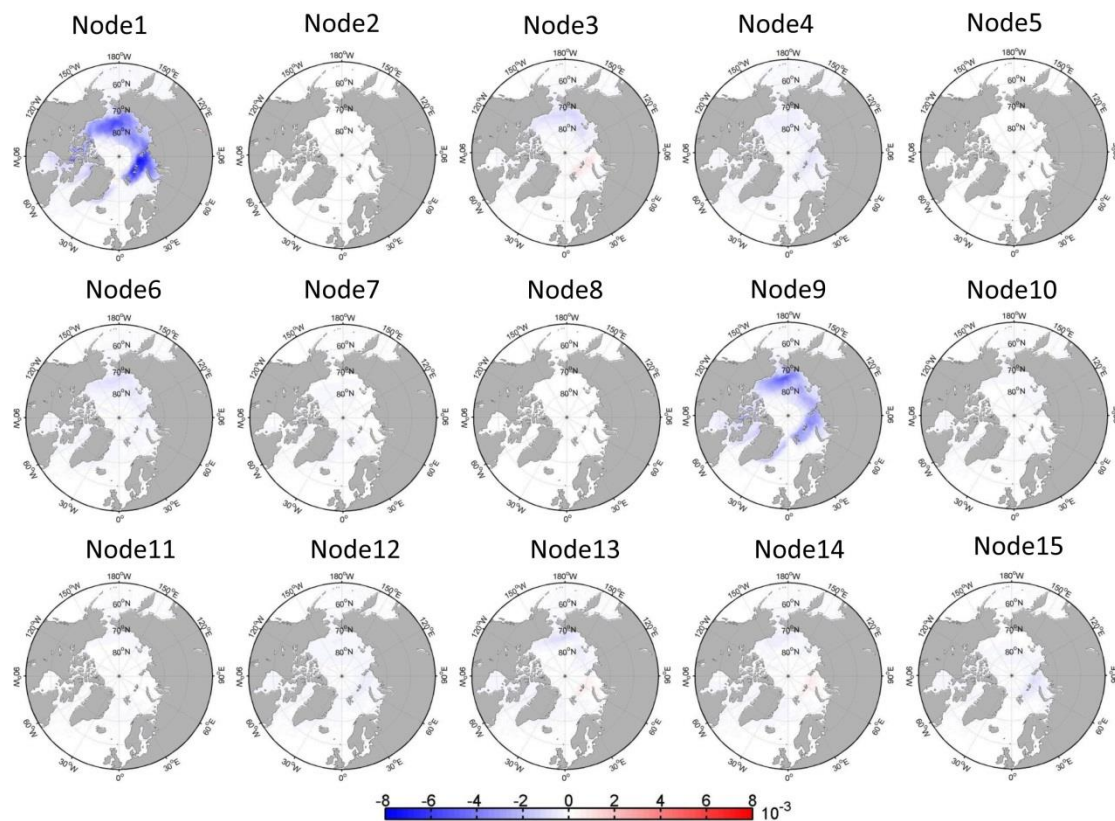Figure S5. Occurrence time series for each SOM pattern in Figure S4.

Figure S6. Trends in the anomalous autumn Arctic sea ice concentration explained by each SOM pattern (Units: yr^{-1}).

2. About reference of previous studies. Although the application of the SOM method to Arctic sea ice is new, some of the results and conclusions drawn from the analysis have been found in previous studies but the authors failed to include them. Some of the relevant studies are listed below -

Gong, T., S. Feldstein, and S. Lee, 2017: The Role of Downward Infrared Radiation in the Recent Arctic Winter Warming Trend. J. Climate, 30, 4937–4949, https://doi.org/10.1175/JCLI-D-16-0180.1

Lee, S., Gong , T., Feldstein, S. B.,Screen, J. A., & Simmonds, I. (2017).Revisiting the cause of the 1989– 2009Arctic surface warming using the sur-face energy budget: Downward infraredradiation dominates the surface ïnˇCˊ uxes.Geophysical Research Letters, 44,10,654–10,661. https://doi.org/10.1002/2017GL075375

I would suggest the authors cite these references and add discussions on the consistency/ inconsistency as compared to previous studies.

Thanks for pointing to these references. We have now added them to section 4 along with some discussion. (lines 177-184)

Gong et al. (2017) and Lee et al. (2017) showed that the increasing downward longwave radiation related to the changes of mid-latitude atmospheric circulation leads to the wintertime Arctic warming. Our focus here is on autumn sea ice trend and we use the low-level water vapour field that is found to resemble more closely to the surface downward radiation fields compared to the total column water (not shown) used in the two studies. Like their studies, the North Atlantic is the main passage of water vapour into the Arctic. But over

the Bering Sea and Europe no water vapour is transported into the Arctic in our studies. Their study period ranges from 1980 to 2010, which is different from our study period (1979-2016).

Minor comments:

Line 36: "natural processes"? why are these processes all natural?

We deleted 'natural'. (line 36)

Lines 40-45: The authors failed to explain the advantages of the SOM method here. The EOF method also provides "a manageable number of representative patterns".

In the third paragraph of the Methods section, we provide the advantages of the SOM over EOF. (lines 88-90)

Line 48: NAO has been defined before

Changed (line 48)

Line 49: ENSO has not been defined

Added (lines 49-50)

Line 80: The authors might want to better define what is "Euclidean distance" in the SOM method

The definition of Euclidean distance has been added. (lines 96-97)

Line 85: smaller number of grids

Changed

Line 86: larger number of grids

Changed

Lines 96-98: The authors should reference Fig. 4a here?

The sentence refers to Figure 1.

Line 134 and 152: It's not easy to tell that it is zonal wave number 2 here.

Changed

Line 193: "decadal-scale natural climate variability to Arctic climate change", why the authors concluded natural here? Can't the SOM nodes include anthropogenic components too?

'natural climate variability' has been changed into 'SST variability'. (line 257)

Fig. 4: I don't see dots in (a)?

Dots are enlarged.

Changes in sea-surface temperature and atmospheric circulation patterns associated with reductions in Arctic sea-ice cover in recent decades

Lejiang Yu[1], Shiyuan Zhong[2]

[1]SOA Key Laboratory for Polar Science, Polar Research Institute of China, Shanghai, China

[2]Department of Geography, Environment and Spatial Sciences, Michigan State University, East Lansing, MI, USA

Correspondence to: Dr. Shiyuan Zhong (zhongs@msu.edu)

Abstract. In recent decades, the Arctic sea ice has been declining at a rapid pace as the Arctic is warmed at a rate of twice the global average. The underlying physical mechanisms for the Arctic warming and accelerated sea ice retreat are not fully understood. In this study, we apply a relatively novel statistical method called Self-Organizing Maps (SOM) to examine the trend and variability of autumn Arctic sea ice in the past three decades and their relationships to large-scale atmospheric circulation changes. Our statistical results show that the anomalous autumn the Arctic Dipole (AD) (Node 1) and the Arctic Oscillation (AO) (Node 9) could explain in a statistical sense as much as 50% of autumn sea ice decline between 1979 and 2016. The Arctic atmospheric circulation anomalies associated with anomalous sea surface temperature patterns over the North Pacific and North Atlantic influence Arctic sea ice primarily through anomalous temperature and water vapour advection and associated radiative feedback.

1 Introduction

In recent decades, the Arctic sea ice has been decreasing at an unprecedented rate (Rothrock et al., 1999; Parkinson, 2014). The accelerated retreat in Arctic sea ice exerts a significant impact not only on the marine and terrestrial ecological systems of the Arctic (Post et al., 2013), but also on the environment of the mid latitude (Mori et al., 2014; Kug et al., 2015).

The underline mechanisms for the Arctic sea ice decline remain to be a subject of active research. Studies have suggested that both anthropogenic forcing due to greenhouse gas and aerosol emissions (Min et al., 2008; Notz and Marotzke, 2012; Gagné et al., 2015) and natural mechanisms at a wide range of scales contribute to the observed Arctic sea ice decline. Local processes, including surface thermal inversion (Bintanja et al., 2011), atmospheric lapse-rate (Pithan and Mauritsen, 2014), ice-albedo feedback (Flanner et al., 2011) and water vapour and cloud radiative feedback (Sedlar et al., 2011), have been found to affect Arctic sea ice. On the other end, global sea-surface temperature (SST) and pressure oscillations, such as the Arctic Dipole (AD) (Wang et al., 2009), the Atlantic Multidecadal Oscillation (AMO) (Park and Latif, 2009), the Arctic Oscillation (AO) (Rigor et al., 2002; Deser and Teng, 2008), the North Atlantic Oscillation (NAO) (Koenigk et al., 2009), and the Pacific Decadal Oscillation (PDO) (Ding et al., 2014), have also been linked to the Arctic sea ice variations and the recent declining trend. Understanding the relative contributions from these multi-scale natural processes to Arctic sea ice decline is vital not only for forecasting sea ice conditions but also for projecting climate change and its impact on the Arctic environment and beyond (Stroeve et al., 2007; Day et al., 2012; Swart et al., 2015;

Ding et al., 2017).

40   In this study, we examine the contributions of changes in large-scale atmosphere and ocean circulations to the trends in Arctic sea ice by applying the Self Organizing Maps (SOM) method (Kohonen, 2001). A relatively new neural network-based method, SOM is superior to some other feature-extracting or clustering methods in that it describes the continuum of atmospheric and oceanic states with a manageable number of representative patterns as compared to only providing useful information on

45 aggregate patterns by Empirical Orthogonal Function (EOF) and other similar methods. Over the past decade, SOM has been widely used in atmosphere and ocean sciences (Hewitson and Crane, 2002; Leloup et al., 2007; Johnson et al., 2008; Lee et al., 2011; Chu et al., 2012). For example, SOM was used to explain the eastward shift of ~~the North Atlantic Oscillation~~ (NAO~~)~~ since the late 1970s (Johnson et al., 2008). The SOM approach was also used to examine the contributions of different El Niño Southern

50 Oscillation (ENSO~~)~~ ~~flavours~~ to the SST trend in the tropical Pacific Ocean (Johnson, 2013).

    We apply SOM to a monthly sea ice concentration dataset for the period 1979 - 2016. We will show how much the recent declining trend in the Arctic sea ice concentrations may be associated with the low frequency atmospheric circulation modes related to SST anomalies over the Pacific and Atlantic Oceans. Although the analyses have been carried out for all four seasons, we will show the results for autumn

55 only since Arctic sea ice reduction in autumn has strongest influence on the wintertime atmospheric circulations over Eurasia and North America (Francis et al., 2009; Petoukhov and Semenov, 2010; Peings and Magnusdottir, 2014).

2 Methods

The period of this study is from 1979-2016. The Arctic sea ice anomaly analysis utilizes the monthly sea

60 ice concentration dataset produced by the United States National Snow and Ice Data Centre (NSIDC) (http://nsidc.org/data/NSIDC-0051). The NSIDC data are on a horizontal grid of 25 km $\times$25 km with a polar stereographic projection. The corresponding SST patterns are analyzed using the $1\degree$ latitude $\times 1\degree$ longitude SST data from the Hadley Centre (Rayner et al., 2003) (http://www.metoffice.gov.uk/hadobs/hadisst/). The SST anomaly patterns are linked to well-known

65 modes of climate variability characterized by several climate indices including the Pacific Decadal Oscillation (PDO) (Mantua et al., 1997) defined as the first EOF mode of SST anomalies in the North Pacific Ocean, the Atlantic Multidecadal Oscillation (AMO) (Enfield et al., 2001) defined as the

3

10-year running mean of detrended SST anomalies in the Atlantic Ocean north of the equator, and the Arctic Oscillation (AO) and Arctic Dipole (AD) defined as the first and second EOF modes of the 1000-hPa geopotential height anomalies north of 70°N (Wang et al., 2009).

The atmospheric circulations are determined using data from the 1.5 $^{\circ}$latitude $\times$ 1.5 $^{\circ}$longitude European Centre for Medium-Range Weather Forecasts (ECMWF) Reanalysis (ERA-Interim) (Dee et al., 2011). Serreze et al. (2012) assessed humidity data from ERA-Interim reanalyses and found only small bias of less than 8% at 1000 hPa for boreal autumn and smaller bias above 1000 hPa. Ding et al. (2017) showed that the ERA-Interim reanalyses can represent reliably the observed circulation, radiation flux, temperature, and water vapour. The surface and upper-air atmospheric variables examined in this study are all extracted from ERA-Interim, except for outgoing long-wave radiation (OLR) that is obtained from the gridded monthly OLR data produced by the US National Oceanic and Atmospheric Administration (NOAA) (http://www.esrl.noaa.gov/psd/data/gridded/data.interp_OLR.html) (Liebmann and Smith, 1996).

The SOM technique is utilized to extract patterns of Arctic sea ice concentrations. A neural network-based method, SOM uses unsupervised learning to determine generalized patterns in complex data. The technique can reduce multidimensional data into two-dimensional array consisting of a matrix of nodes. Each node in the array has a reference vector that displays a spatial pattern of the input data. All patterns in the two-dimensional array represent the full continuum of states in the input data. The SOM algorithm also is a clustering technique, but unlike other clustering technique, it does not need a priori decisions on data distribution. Unlike the EOF analysis, the SOM technique does not require the orthogonality of two spatial patterns. A detailed description of the SOM algorithm can be found in Kohonen (2001).

In this study, the SOM technique is used to categorize anomalous seasonal sea ice concentration patterns north of 50°N for autumn (September-October-November). Seasonal anomalies are calculated by subtracting the climatology for the season relative to the study period 1979-2016 from the seasonal means. The anomalous sea ice pattern for each autumn is assigned to the best-matching SOM pattern on the basis of minimum Euclidean distance, a measure of straight-line distance between two points in Euclidean space and calculated by the product of root-mean-square error and the square root of the number of grid points. Spatial correlations between sea ice field for each autumn and its corresponding

4

best-matching SOM pattern are calculated and the overall mean spatial correlation coefficients obtained by averaging over the 38 autumns are used to determine the number of SOM nodes or grids to be used in the current analysis (Lee and Feldstein, 2013). Table 1 shows the overall mean spatial correlation coefficients for several SOM grid configurations with nodes ranging from 2×2 to 4×5. As expected, the overall correlation increases as the number of nodes increases. The largest jump between any two grid configurations occurs from a 2×4 grid to a 3×3 grid. Thus, a 3×3 grid is selected for the SOM analysis. While a higher spatial correlation can be achieved with larger number of grids, the 3x3 grid is able to capture the main variability pattern in the autumn Arctic sea ice at the sacrifice of some details that can be depicted by larger number of grids. The frequency of occurrence for each SOM node is defined as the number of autumns that node represents divided by the total number of autumns (38) in the study period. The contribution of each SOM pattern to the trends in the Arctic sea ice concentrations is calculated by the product of each SOM pattern and a rate determined by temporal linear regression of the number of the projections of each pattern for each autumn (Johnson, 2013). The sum of these contributions presents the trends in Arctic sea ice explained in the statistical sense by the SOM patterns, which in this case indicates trends resulting from low-frequency variability. The significance of the trends in the time series for each SOM pattern is tested using the Student's t-test. Residual trends are calculated by subtracting SOM-explained trends from the total trends.

3 SOM results

Sea ice concentration anomalies occur mainly in the marginal seas from the Barents Sea to the Beaufort Sea, with maximum anomalies in the Barents Sea and the Kara Sea, and over the Beaufort Sea and the East Siberian Sea (Fig. 1). Nodes 1, 2 and 4 depict all negative anomalies, whereas Nodes 5, 6, 8 and 9 exhibit all positive anomalies. Nodes 3 and 7, on the other hand, show a mixed pattern with opposite changes in the Barents Sea in the Atlantic sector of the Arctic Ocean and the Beaufort Sea and East Siberian Sea over the Pacific sector. The largest change with similar strength over the Pacific and the Atlantic sectors are depicted by Nodes 1 and 9, and both nodes also have the highest (24%) frequency of occurrences. The other nodes that are either all positive or all negative exhibit larger spatial variability in the strengths of the signals with much stronger signal in either the Atlantic sector (Nodes 2, 5 and 8) or the Pacific sector (Nodes 4 and 6). The two mixed patterns show similar strength over the two sectors, but the pattern with positive anomalies over the Beaufort Sea and the East Siberian Sea and negative

5

anomalies over the Barents Sea, as depicted by Node 3, occurs much more frequently (13%) than the opposite pattern represented by Node 7 (8%).

The trends in the frequency of occurrence for each SOM pattern and their contribution to the trends in the Arctic autumn sea ice concentrations are examined and the results are shown in Fig. 2. The nodes with spatially uniform changes appear to be separated into two clusters with those showing all positive anomalies (Nodes 5, 6, 8 and 9) appearing in the 80s and 90s and those having all negative anomalies (Nodes 1 and 4) appearing after 2000. The transition from all positive anomalies in the earlier part, to all negative anomalies in the later part, of the time series is consistent with the trends in the observed Arctic sea ice concentration during the same time period. Not surprisingly, the transition appears to be dominated by the two strongest and most frequent patterns denoted by Node 9 (all positive and occurring from the 1980s through mid 1990s) and Node 1 (all negative and occurring exclusively after 2005). Only these two nodes have linear trends that are statistically significant at above 95% confidence level. The slopes of the trend lines for these two nodes are opposite but the values are similar (0.027 yr^{-1} for Node 1 and -0.021 yr^{-1} for Node 9). The other nodes have statistically insignificant trends with magnitudes less than 0.01 yr^{-1}.

The spatial patterns of the autumn sea ice concentration trends explained in a statistical sense by each node and by all nodes are shown in Figs. 3 and 4. Together, the nine SOM nodes explain statistically about 60% of total trends in the autumn sea ice loss (Fig. 4b). Among them Node 1 explains statistically the largest portion (33%) of the total trend, followed by Node 9 (21%), with the other 7 nodes together accounting for only 6% of the loss.

For comparison, the SOM patterns and their occurrence time series for a larger grid (3x5) are provided in Supplement (Figs. S1 and S2). As expected, with more nodes, the 3x5 grid depict more details and each node has smaller frequency compared to the 3x3 grid. However, the dominant nodes (also nodes 1 and 9) show nearly identical patterns as those in the 3x3 grid. Like the 3×3 grid, nodes 1 and 9 in the 3×5 grid make greater contributions to the trend in autumn Arctic sea ice than other nodes (Fig. S3). Also as expected, the trend explained by nodes 1 and 9 in the 3x5 grid is smaller (46%) compared to 54% by the same two nodes in the 3×3 grid.

4 Potential Mechanisms

To explain statistically the spatial patterns depicted by the two dominant nodes, we made composite maps over the years of occurrences for Nodes 1 and 9, respectively, and Figs. 5-7 show composite patterns of the anomalous SST and OLR (as a proxy for tropical convection) and anomalous atmospheric circulations represented by the 500-hPa geopotential height, 850-hPa wind, surface-750-hPa specific humidity, surface downward longwave radiation, and surface air temperature.

For Node 1, the SST composite pattern resembles negative phase of the PDO in the North Pacific and positive phase of the AMO in the North Atlantic (Fig. 5). The positive SST anomalies over the tropical western Pacific produce anomalous local convection, exciting a wave train (Hoskins and Karoly, 1981; Jin and Hoskins, 1995; Higgins and Mo, 1997), which propagates northeastwards to North Pacific, North America, North Atlantic, and Eurasia (Fig. 5). In mid-latitudes, the anomalous SST and the nodes of the wave train interacts to produce atmospheric circulation anomalies. Over the Arctic, the SST and height patterns are similar to those associated with a negative phase AD, with a negative 500-hPa height anomaly center over Greenland and the Baffin Bay, and a positive anomaly center over the Kara Sea. The zonal pressure gradient between the two centers induces anomalous low-troposphere southwesterly and southerly winds over the North Atlantic Ocean (Fig. 6) that transport warm and moist air from North Atlantic into the Arctic Ocean north of Eurasia, thus increasing surface air temperature and humidity and reducing sea ice concentration in the Arctic (Fig. 7). The higher moisture content in the Arctic surface air also facilitates the occurrence of water vapour and cloud radiative feedback process (Sedlar et al., 2011) during which increased downward longwave radiation (Fig. 7) enhances surface warming and sea ice melting. The anomalous high pressure produces subsidence and the adiabatic warming associated with the sinking air contributes to the sea ice loss (Ding et al., 2017) (Not shown). The opposite may occur in the region under the anomalous low pressure center. But the warm southwesterly winds over the northeastern Canada also favor the sea ice loss there. Gong et al. (2017) and Lee et al. (2017) showed that the increasing downward longwave radiation related to the changes of mid-latitude atmospheric circulation leads to the wintertime Arctic warming. Our focus here is on autumn sea ice trend and we use the low-level water vapour field that is found to resemble more closely to the surface downward radiation fields compared to the total column water (not shown) used in the two studies. Like their studies, the North Atlantic is the main passage of water vapour into the Arctic. But over the Bering Sea

and Europe no water vapour is transported into the Arctic in our studies. Their study period ranges from 1980 to 2010, which is different from our study period (1979-2016).

For Node 9, the SST composite is characterized by negative anomalies in both the Pacific and the Atlantic except for areas of the tropical Pacific and the west coast of North America (Fig.5). The negative SST anomalies over the tropical western Pacific, corresponding to suppressed convective activities, generate one wave train that is in opposite phase to the wave train associated with Node 1. Similarly, the nodes of the wave train interact with the local SST anomalies over the mid-latitude regions, producing a nearly opposite (but not symmetrical) anomalous atmospheric circulation pattern to that of Node 1.   Over the Arctic, the patterns resemble a positive phase AO (Fig.5). Anomalous northeasterly winds in the North Atlantic Ocean induced by anomalous Icelandic low are unfavourable for warm air intrusion into the Arctic Ocean (Fig. 6), a result also indicated in a previous study (Kim et al., 2017). Despite the occurrences of anomalous southwesterly winds over the Barents Sea and southeasterly winds over the Sea of Okhotsk, the cold advection from anomalous cold sea water prevents the Arctic sea ice from melting. Meanwhile the cold advection also reduces water vapor content in the lower troposphere and the resulting smaller downward longwave radiation facilitates the occurrence of negative surface air temperature and positive Arctic sea ice anomalies north of Eurasia (Fig. 7). The northerly winds over the Beaufort Sea, northeastern Canada and Greenland Sea also contribute to the decrease in surface air temperature and increase in the sea ice concentration.

The opposite patterns in Nodes 1 and 9 can be largely associated with the differences in the water vapor-radiation feedback process resulting from anomalous temperature and especially water vapour transport by anomalous atmospheric circulations associated with different patterns of SST anomalies over the North Pacific and Atlantic. The patterns of SST anomalies are nearly symmetric for the two nodes over the North Atlantic, but they are somewhat asymmetric over the North Pacific. For Node 1, there is one center of high SST over the central North Pacific, whereas Node 9 is associated with two centers of low SST: one over the Coast of Japan and another in central North Pacific. These differences in the SST anomaly patterns lead to different wave trains and high-latitude atmospheric circulations.

For the composite analysis often used in previous literature, lower (higher) Arctic sea concentration years refer to after (before) 2000.

The SOM-based composites in the above discussion, which are made using years indicated (Fig. 2) by the occurrences for Node 1 (2007-2013, 2015-2016), and, separately, for node 9 (1980-1982,

8

1986-1989, 1992, 1996), are compared to composites of years of high (before 2000) and low (after 2000) Arctic sea ice coverage according to the Autumn Arctic sea ice time series (Figure 8). The composited SST patterns over the North Pacific are almost a mirror image to each other, indicating a positive (negative) phase PDO before (after) 2000 (Fig. 8). On the other hand, the composited SST patterns corresponding to Node 1 and Node 9 are not symmetrical (Fig. 5). Similar situations occur over North Atlantic. The magnitude and significant level of SOM-based SST composites in Fig. 5 are also higher than the time-series-based composites in Fig. 8. Similarly, in mid-latitudes, the composites of the anomalous 500hPa geopotential heights before and after 2000 are nearly symmetrical (Fig. 8) and the significant level and amplitude of the wave train are also lower than those in Fig. 5. At high latitudes, the anomalous atmospheric circulations in Fig. 8 show a mixed pattern of AO and AD and have no extreme centers. However, Fig. 5 exhibits clear AO and AD patterns and extreme centers, revealing more clearly the relationship between the anomalous sea ice concentration and anomalous atmospheric circulations. Based on these examples, the SOM-based composites allows for better depiction of atmospheric and SST conditions corresponding to sea ice anomaly patterns compared to typical time-series-based composite approach.

One drawback of the SOM-based composite is the relatively small number of composite members (Node 1 and Node 9 each has 9 members), which makes the composite more vulnerable to the influence of extreme cases. To examine this issue, the standard deviations of the SOM-based composites are compared to those of time-series-based composites that have much larger members (17 members for after-2000- composites and 21 members for before-2000-composites) and the results for the anomalous SST and 500-hPa height are shown in Figs. S4 and S5. The spatial patterns and magnitudes of the standard deviations are similar between the Node-1 and after-2000 composites and between Node-9 and before-2000 composites. The F-test indicates that except for small patches there are no statistically significant differences in the standard deviations between the small member SOM-based composites and the large-member typical composites (Fig. S6), suggesting it is unlikely the SOM-based composites are strongly influenced by extreme cases as a result of small composite members.

9

5 Conclusions

We investigate the potential mechanisms for the autumn arctic sea ice decline for the period 1979-2016 using the SOM method. Our results show that more than half of the autumn Arctic sea ice loss may be associated with the changes in the temperature and water vapour transport and the associated water vapour radiation feedback resulting from anomalous atmospheric circulations linked to SST anomalies over the North Pacific and North Atlantic. This result provides further evidence that the mid-latitude SST anomalies play a vital role in the accelerated Arctic sea ice decline in recent decades (Ding et al., 2017; Yu et al., 2017). The main result is that the opposite pattern of the Arctic sea ice anomalies during the early (positive) and later (negative) parts of the 1979-2016 period is not associated with opposite phase of an atmospheric circulation mode, but instead the change can be largely associated with two different atmospheric circulation patterns (AO and AD) associated with an asymmetry in the anomalous SST distributions over the North Pacific. The teleconnections between the Arctic sea ice variability and mid-latitude SST anomalies suggest that on a decadal or longer time scale it may be necessary to include the Arctic sea ice and mid-latitude SST interactions or feedbacks in any investigations of Arctic warming and sea ice decline and their potential influence on mid-latitude weather and climate, an area of active research in recent years (Barnes and Screen, 2015; Overland and Wang, 2015; Francis and Skific, 2015). Finally, the results here help advance the knowledge about the relatively large contributions from the decadal-scale ~~natural climate~~SST variability to Arctic climate change, though further studies using coupled global atmosphere-ocean-sea ice models are warranted to fully understand the physical mechanisms.

Data Availability

All data used in the current study are publicly available. The monthly sea ice concentration data are available from the National Snow and Ice Data Center (NSIDC) (http://nsidc.org/data/NSIDC-0051), the ERA-Interim reanalysis data are available from the European Center for Mid-Range Weather Forecasting (https://www.ecmwf.int/en/forecasts/datasets/reanalysis-datasets/era-interim) and the SST data are available from the Hadley Centre for Climate Prediction and Research (http://www.metoffice.gov.uk/hadobs/hadisst/).

Competing interests

The authors declare that they have no conflict of interest.

Author Contributions

L. Yu designed the study, with input from S. Zhong, and carried out the analyses. L. Yu and S. Zhong prepared the manuscript.

Acknowledgements

References

Barnes, E. A., and Screen, J.: The impact of Arctic warming on the midlatitude jet stream: Can it? Has it? Will it? WIREs Clim. Change, 6, 277-286,   https://doi.org/10.1002/wcc.337, 2015.

Bintanja, R., Graversen, R. G., and Hazeleger, W.: Arctic winter warming amplified by the thermal inversion and consequent low infrared cooling to space, Nat. Geosci., 4, 758-761, https://doi.org/10.1038/ngeo1285, 2011.

Chu, J.-E., Hameed, S. N., and Ha, K.-J.: Non-linear intraseasonal phases of the East Asian summer monsoon: Extraction and analysis using self-organizing maps, J. Climate, 25, 6975-6988, https://doi.org/10.1175/JCLI-D-11-00512.1, 2012.

Day, J. J., Hargreaves, J. C., Annan, J. D., and Abe-Ouchi, A.: Sources of multidecadal variability in Arctic sea ice extent, Environ. Res. Lett., 7, 034011, https://doi.org/10.1088/1748-9326/7/7/034011, 2012.

Dee, D. P., Uppala, S. M., Simmons, A. J., Berrisford, P., Poli, P., Kobayashi, S., Andrae, U., Balmaseda, M. A., Balsamo, G., Bauer, P., Bechtold, P., Beljaars, A. C. M., van de Berg, L., Bidlot, J., Bormaan, N., Delsol, C., Dragani, R., Fuentes, M., Geer, A. J., Haimberger, L., Healy, S. B., Hersbach, H., Hólm, E. V., Isaksen, L., Kållberg, P., Köhler, M., Matricardi, M., McNally, A. P., Mong-Sanz, B. M., Morcrette, J.-J., Park, B.-K., Peubey, C., de Rosnay, P., Tavolato, C., Thépaut, J.-N., and Vitart, F.: The ERA-Interim reanalysis: configuration and performance of the data assimilation system, Q. J. R. Meteorol. Soc., 137, 553-597, https://doi.org/10.1002/qj.828, 2011.

Deser, C., and Teng, H.: Evolution of Arctic sea ice concentration trends and the role of atmospheric

295   circulation forcing, Geophys. Res. Lett., 35, L02504, https://doi.org/10.1029/2007GL032023, 2008.

Ding, Q., Wallace, J. M., Battisti, D. S., Steig, E. J., Gallant, A. J. E., Kim, H.-J., and Geng, L.: Tropical forcing of the recent rapid Arctic warming in northeastern Canada and Greenland, Nature, 509, 209–212, https://doi.org/10.1038/nature13260, 2014.

300   Ding, Q., Schweiger, A., L'Heureux, M., Battisti, D. S., Po-Chedley, S., Johnson, N. C., Blanchard-Wrigglesworth, E., Harnos, K., Zhang, Q., Eastman, R., and Steig, E. J.: Influence of high-latitude atmospheric circulation changes on summertime Arctic sea ice, Nat. Clim. Change, 7, 289-295, https://doi.org/10.1038/NCLIMATE3241, 2017.

Enfield, D. B., Mestas-Nunez, A. M., and Trimble, P. J.: The Atlantic Multidecadal Oscillation and its

305   relationship to rainfall and river flows in the continental US, Geophys. Res. Lett., 28, 2077–2080, https://doi.org/10.1029/2000GL012745, 2001.

Flanner, M. G., Shell, K. M., Barlage, M., Perovich, D. K., and Tschudi, M. A.: Radiative forcing and albedo feedback from the Northern Hemisphere cryosphere between 1979 and 2008, Nat. Geosci., 4, 151–155, https://doi.org/10.1038/NGEO1062, 2011.

310   Francis, J. A., Chan, W., Leathers, D. J., Miller, J. R., and Veron, D. E.: Winter Northern Hemisphere weather patterns remember summer Arctic sea-ice extent, Geophys. Res. Lett., 36, L07503, https://doi.org/10.1029/2009GL037274, 2009.

Francis, J. A., and Skific, N.: Evidence linking rapid Arctic warming to mid-latitude weather patterns, Phil. Trans. R. Soc. A., 373, 20140170, https://doi.org/10.1098/rsta.2014.0170, 2015.

315   Gagné, M. –È., Gillett, N. P., and Fyfe, J. C.: Impact of aerosol emission controls on future arctic se ice cover, Geophys. Res. Lett., 42, 8481-8488, https://doi.org/10.1002/2015GL065504, 2015.

Gong, T., Feldstein, S., and Lee, S.: The Role of Downward Infrared Radiation in the Recent Arctic Winter Warming Trend. J. Climate, 30, 4937–4949, https://doi.org/10.1175/JCLI-D-16-0180.1, 2017.

320   Hewitson, B. C., and Crane, R. G.: Self-organizing maps: Applications to synoptic Climatology, Clim. Res., 22, 13-26, 2002.

Higgins, R. W., and Mo, K. C.: Persistent North Pacific circulation anomalies and the tropical intraseasonal circulation, J. Climate, 10, 223-244, 1997.

Hoskins, B. J., and Karoly, D. J.: The steady linear response of a spherical atmosphere to thermal and

325   orographic forcing, J. Atmos. Sci., 38, 1179-1196.

Jin, F., and Hoskins, B. J.: The direct response to tropical heating in a baroclinic atmosphere, J. Atmos.

Sci., 50, 1661-1671, https://doi.org/10.1175/1520-0469(1995)052<0307:TDRTTH>2.0.CO;2,

1995.

Johnson, N. C., Feldstein, S. B., and Tremblay, B.: The continuum of Northern Hemisphere

330   teleconnection patterns and a description of the NAO shift with the use of self-organizing maps, J.

Climate, 21, 6354-6371, https://doi.org/10.1175/2008JCLI2380.1, 2008.

Johnson, N. C.: How many ENSO flavors can we distinguish?, J. Climate, 26, 4816-4827,

https://doi.org/10.1175/JCLI-D-12-00649.1, 2013.

Kim, B.-M., Hong, J.-Y., Jun, S.-Y., Zhang, X., Kwon, H., Kim, S.-J., Kim, J.-H., Kim, S.-W., and

335   Kim, H.-K.: Major cause of unprecedented arctic warming in January 2016: Critical role of an

Atlantic windstorm, Sci. Rep., 7, 40051, https://doi.org/10.1038/srep40051, 2017.

Koenigk, T., Mikolajewicz, U., Jungclaus, J., and Kroll, A.: Sea ice in the Barents Sea: Seasonal to

interannual variability and climate feedbacks in a global coupled model, Clim. Dyn., 32,

1119–1138, https://doi.org/10.1007/s00382-008-0450-2, 2009.

340 Kohonen, T. (Eds): Self-organizing maps, 3rd ed. Springer, Berlin, Germany, 501pp., 2001.

Kug, J.-S., Jeong, J.-H., Jang, Y.-S., Kim, B.-M., Folland, C. K., Min, S.-K., and Son, S.-W.: Two

distinct influences of Arctic warming on cold winters over North America and East Asia, Nat.

Geosci., 8, 759-762, https://10.1038/NGEO2517, 2015.

Lee, S., and Feldstein, S. B.: Detecting ozone-and greenhouse gas-driven wind trends with observational

345   data, Science, 339, 563-567, https://doi.org/10.1126/science.1225154, 2013.

Lee, S. T., Gong, T., Johnson, N. C., Feldstein, S. B., and Polland, D.: On the possible link between

tropical convection and the Northern Hemisphere Arctic surface air temperature change between

1958 and 2001, J. Climate, 24, 4350-4367, https://doi.org/10.1175/2011JCLI4003.1, 2011.

Lee, S., Gong , T., Feldstein, S. B., Screen, J. A., and Simmonds, I.: Revisiting the cause of the 1989-

350   2009Arctic surface warming using the surface energy budget: Downward infrared radiation

dominates the surface fluxes. Geophysical Research Letters, 44, 10654–10661.

https://doi.org/10.1002/2017GL075375, 2017.

Leloup, J., Lachkar, Z., Boulanger, J.-P., and Thiria, S.: Detecting decadal changes in ENSO using

neural networks, Clim. Dyn., 28, 147-162, https://10.1007/s00382-006-0173-1, 2007.

355   Liebmann, B., and Smith, C.A.: Description of a Complete (Interpolated) Outgoing Longwave Radiation

Dataset, *Bulletin of the American Meteorological Society*, **77**, 1275-1277, 1996.

Mantua, N. J., Hare, S. R., Zhang, Y., Wallace, J. M., and Francis, R. C.: A Pacific interdecadal climate

oscillation with impacts on salmon production, Bull. Am. Meteorol. Soc., 78, 1069–1079,

https://10.1175/1520-0477(1997)078<1069:APICOW>2.0.CO;2 , 1997.

360   Min, S.-K., Zhang, X., Zwiers, F. W., and Agnew, T.: Huamn influence on arctic sea ice detectable from

early 1990s onwards, Geophys. Res. Lett., 35, 213-36, https://10.1029/2008GL035725, 2008.

Mori, M., Watanabe, M., Shiogama, H., Inoue, J., and Kimoto, M.: Robust Arctic sea-ice influence on

the frequent Eurasian cold winters in past decades, Nat. Geosci., 7, 869-873,

https://doi.org/10.1038/NGEO2277, 2014.

365   Notz, D., and Marotzke, J.: Observations reveal external driver for Arctic sea-ice retreat, Geophys. Res.

Lett., 39, 89-106, https://doi.org/10.1029/2012GL051094, 2012.

Overland, J. E., and Wang, M.: Increased variability in the early winter subarctic North American

atmospheric circulation, J. Climate, 28, 7297-7305,

https://doi.org/10.1175/JCLI-D-15-0395.1,2015.

370   Park, W., and Latif, M.: Multidecadal and multicentennial variability of the meridional overturning

circulation, Geophys. Res. Lett., 35, L22703, https://doi.org/10.1029/2008GL035779, 2008.

Parkinson, C. L.: Global sea ice coverage from satellite data: Annual cycle and 35-Yr trends, J. Climate,

27, 9377–9382, https://doi.org/10.1175/JCLI-D-14-00605.1, 2014.

Peings, Y., and Magnusdottir, G.: Response of the wintertime Northern Hemisphere atmospheric

375   circulation to current and projected Arctic sea ice delcine: a numerical study with CAM5, J.

Climate, 27, 244-264, https://doi.org/10.1175/JCLI-D-13-00272.1, 2014.

Petoukhov, V., and Semenov, V. A.: A link between reduced Barents-Kara sea ice and cold winter

extremes over northern continents, J. Geophys. Res., 115, D211111,

https://doi.org/10.1029JD013568, 2010.

380   Pithan, F., and Mauritsen, T.: Arctic amplification dominated by temperature feedbacks in contemporary

climate models, Nat. Geosci., 7, 181-184, https://doi.org/10.1038/NGEO2071, 2014.

Post, E., Bhatt, U. S., Bitz, C. M., Brodie, J. F., Fulton, T. L., Hebblewhite, M., Kerby, J., Kutz, S. J.,

Stirling, I., and Walker, D. A.: Ecological consequences of sea-ice decline, Science, 341,

519–524, https://doi.org/10.1126/science.1235225, 2013.

385   Rayner, N. A., Parker, D. E., Horton, E. B., Folland, C. K., Alexander, L. V., Rowell, D. P., Kent, E.

          C., and Kaplan, A.: Global analyses of sea surface temperature, sea ice, and night marine air

          temperature since the late nineteenth century, J. Geophys. Res., 108, 4407,

          https://doi.org/10.1029/2002JD002670, 2003.

      Rigor, I., Wallace, J. M., and Colony, R. L.: Response of sea ice to the Arctic Oscillation, J. Climate, 15,

390   2648–2663, https://doi.org/10.1175/1520-0442(2002)015<2648:ROSITT>2.0.CO;2, 2002.

      Rothrock, D. A., Yu, Y., and Maykut, G. A.: Thinning of the Arctic sea-ice cover, Geophys. Res. Lett.,

          26, 3469–3472, 1999.

      Sedlar, J., Tjernström, M., Mauritsen, T., Shupe, M. D., Brooks, I. M., Persson, P. Ola G., Birch, C. E.,

          Leck, C., Sirevaag, A., and Nicolaus, M.: A transitioning Arctic surface energy budget: the

395   impacts of solar zenith angle, surface albedo and cloud radiative forcing, Clim. Dyn., 37,

          1643-1660, https://doi.org/10.1007/s00382-010-0937-5, 2011.

      Serreze, M. C., Barrett, A. P., and Stroeve, J.: Recent changes in tropospheric water vapor over the

          Arctic as assessed from radiosondes and atmospheric reanalyses, J. Geophys. Res., 117, D10104,

          doi:10.1029/2011JD017421, 2012.

400   Stroeve, J., Holland, M., Meier, W., Scambos, T., and Serreze, M.: Arctic sea ice decline: Fast than

          forecast, Geophys. Res. Lett., 34, L09501, https://doi.org/10.1029/2007GL029703, 2007.

      Swart, N. C., Fyfe, J. C., Hawkins, E., Kay, J. E., and Jahn, A.: Influence of internal variability on Arctic

          sea-ice trends, Nat. Clim. Change, 5, 86-89, 2015.

      Wang, J., Zhang, J., Watanabe, E., Ikeda, M., Mizobata, K., Walsh, J. E., Bai, X., and Wu, B.: Is the

405   Dipole anomaly a major driver to record lows in Arctic summer sea ice extent?, Geophys. Res.

          Lett., 36, L05706, https://doi.org/10.1029/2008GL036706, 2009.

      Yu, L., Zhong, S., Winkler, J. A., Zhou, M., Lenschow, D. H., Li, B., Wang, X., and Yang, Q.: Possible

          connections of the opposite trends in Arctic and Antarctic sea-ice cover, Sci. Rep., 7, 45804,

          https:// doi.org/10.1038/srep45804, 2017.

410

Table 1. The 38-year (1979-2016) average of spatial correlations between the seasonal Arctic sea ice concentration and the corresponding SOM pattern for each year.

SOM grids	2×2	2×3	2×4	3×3	3×4	3×5	4×4	4×5
Correlation coefficients	0.59	0.56	0.59	0.64	0.66	0.69	0.68	0.70

Figure captions

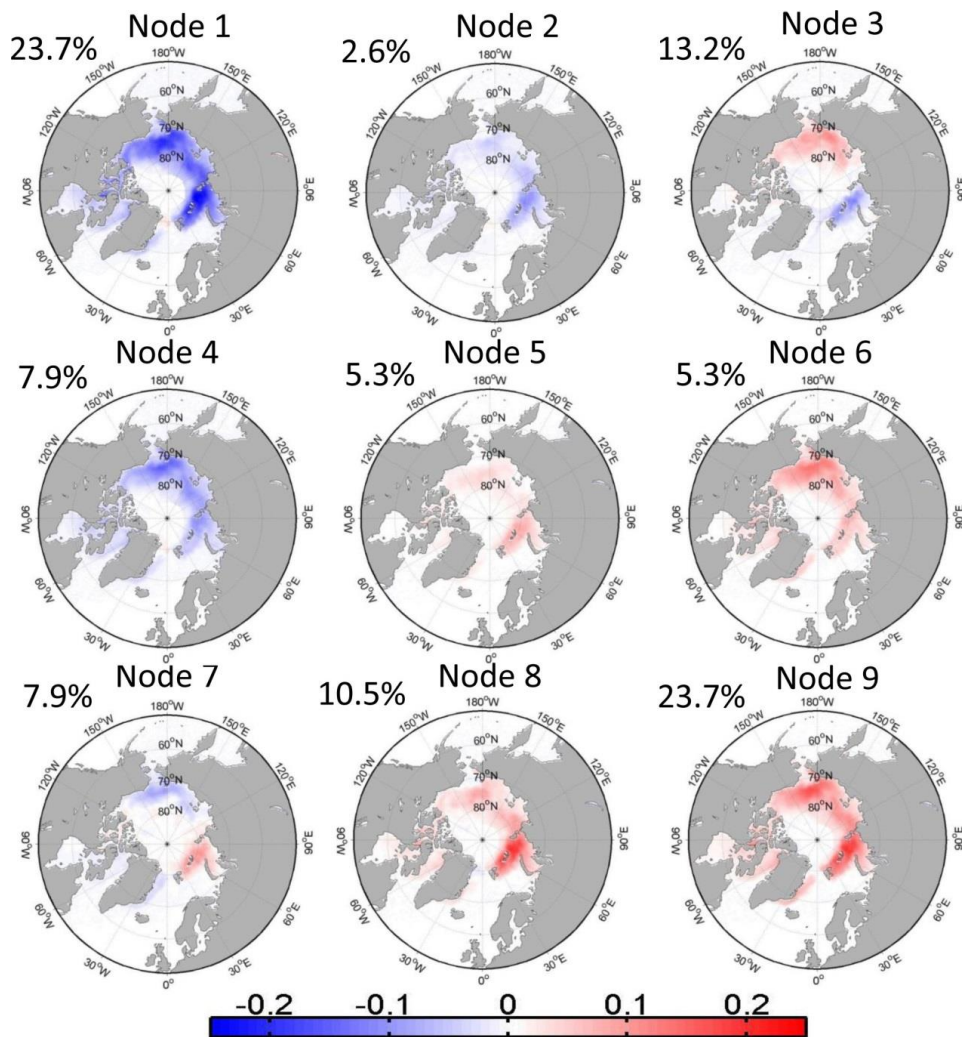Fig.1. The SOM patterns of autumn (September-November) Arctic sea ice concentration for a 3×3 grid for the 1979-2016 period. The percentages at the top left of each panel indicate the frequency of occurrence of the pattern.

Fig. 2. Occurrence time series for each SOM pattern in Fig. 1.

Fig. 3. In the statistical sense, trends in the autumn Arctic sea ice concentration explained by each SOM pattern (Units: yr^{-1}).

Fig. 4. Total (a), SOM-explained (b) and residual (c) autumn Arctic sea ice concentration trends (Units: yr^{-1}). Dots in (a) indicate above 90% confidence level.

Fig. 5. Composites of anomalous sea surface temperature (℃) and 500-hPa geopotential height (gpm) for nodes 1 and 9. Dotted regions denote above 90% confidence level.

Fig. 6. The same as Fig. 5, but for 850-hPa wind field. Shaded regions denote above 90% confidence level.

Fig. 7. The same as Fig. 5, but for integrated atmospheric water vapor from surface to 750 hPa (g kg^{-1}), accumulated surface downward longwave radiation (W $m^{-2} \times 10^5$) and surface air temperature (℃). Dotted regions denote above 90% confidence level.

Fig. 8. Composites of anomalous sea surface temperature (℃) and 500-hPa geopotential height (gpm) for after and before 2000. Dotted regions denote above 90% confidence level.

Figure1 The SOM patterns of the autumn (September-November) Arctic sea ice concentration for a 3×3 grid for the 1979-2016 period. The percentages at the top left of each panel indicate the frequency of occurrence of the pattern.

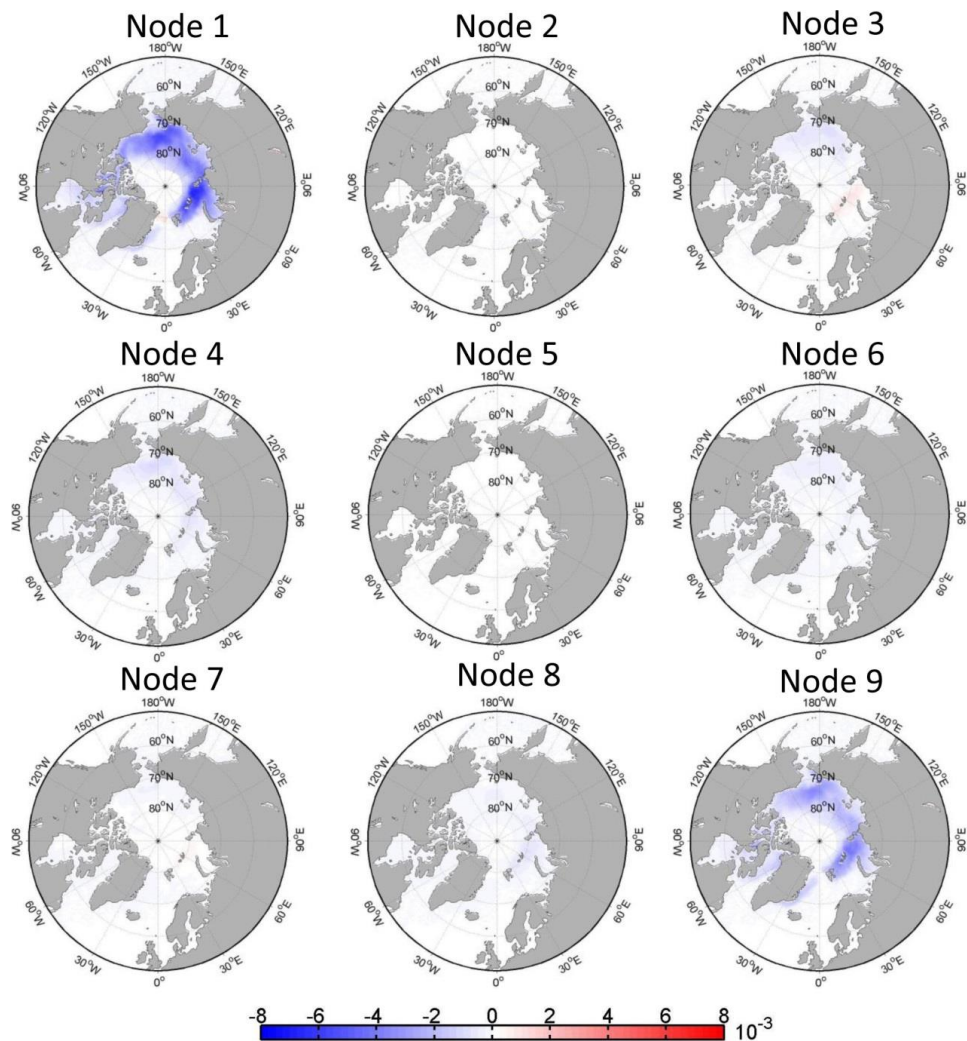Figure 2. Occurrence time series for each SOM pattern in Figure 1.

Figure 3. In the statistical sense, trends in the autumn Arctic sea ice concentration explained by each SOM pattern (Units: yr^{-1}).
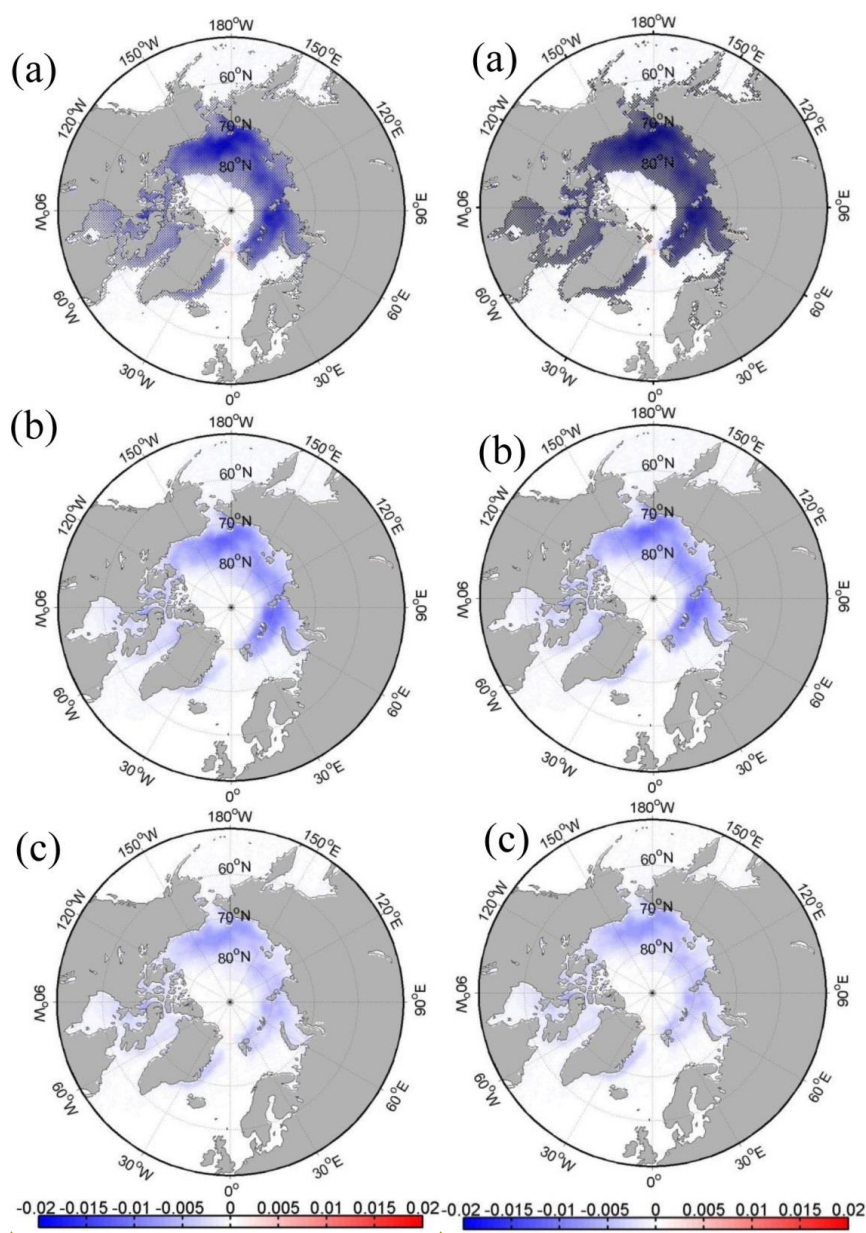
Figure 4. Total (a), SOM-explained (b) and residual (c) autumn Arctic sea ice concentration trends. (Units: yr^{-1}). Dots in (a) indicate above 95% confidence level.
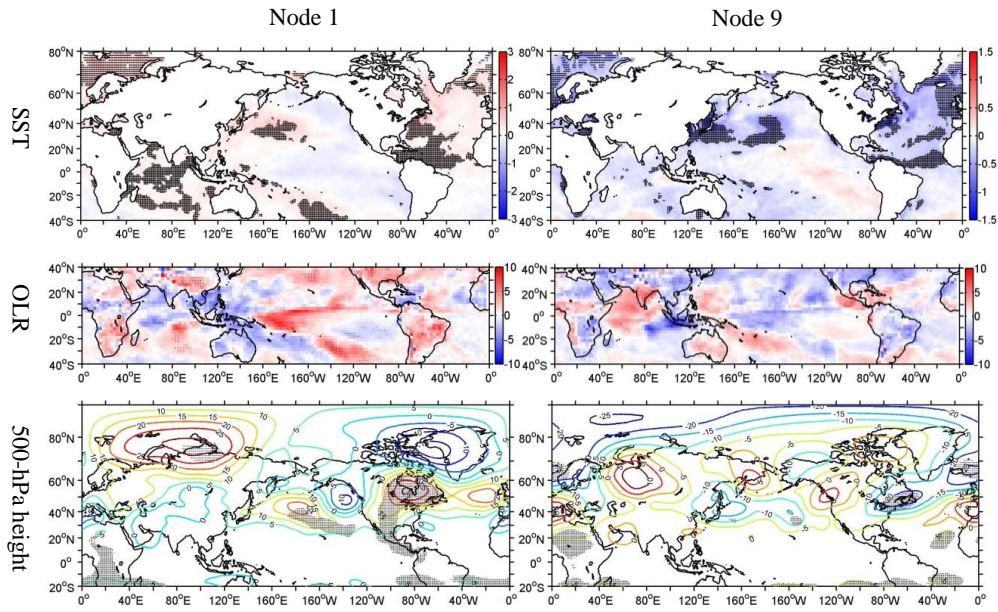
Figure 5. Composites of anomalous sea surface temperature (°C), outgoing long wave radiation (OLR) (W m⁻²) and 500-hPa geopotential height (gpm) for nodes 1 and 9. Dotted regions denote above 90% confidence level.
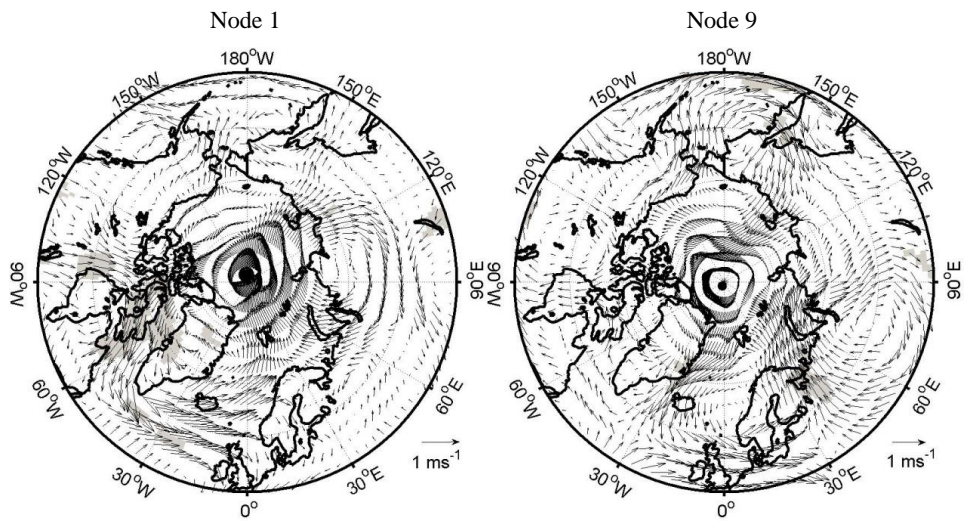
Node 1   Node 9

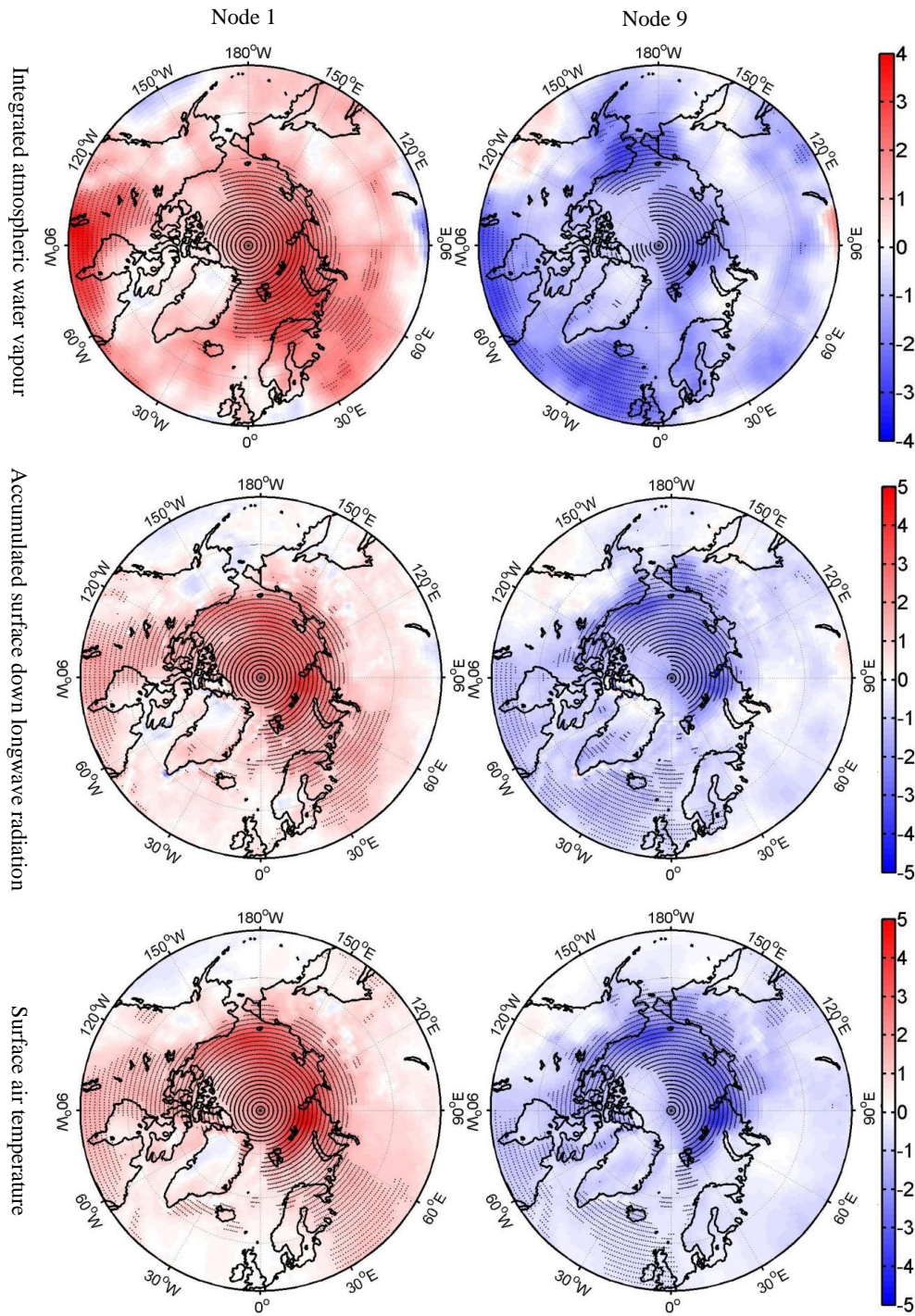Figure 6. The same as Figure 5, but for 850 hPa wind field. Shaded regions denote above 90% confidence level.

Figure 7. The same as Figure 5, but for integrated atmospheric water vapor from surface to 750 hPa (g kg^{-1}), accumulated surface downward longwave radiation (10^{5}Wm^{-2}), and surface air temperature (℃). Dotted regions denote above 90% confidence level.
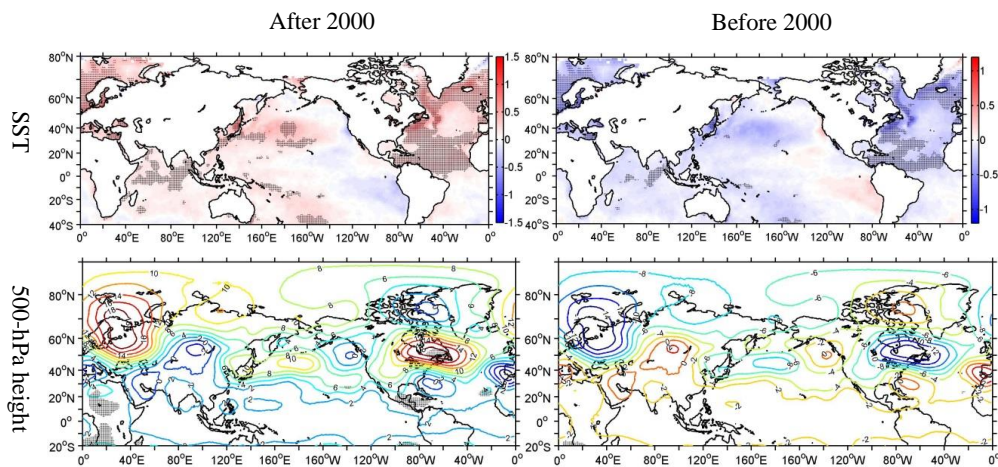
Figure 8. Composites of anomalous sea surface temperature (℃) and 500-hPa geopotential height (gpm) for after and before 2000. Dotted regions denote above 90% confidence level.